Simulation and experimental determination of the online separation of blood components with the help of microfluidic cascading spirals

Lisa Sprenger,[1,2,a)] Silvio Dutz,[3] Thomas Schneider,[4] Stefan Odenbach,[1] and Urs O. Häfeli[2,a)]
[1]*TU Dresden, Institute of Fluid Mechanics, 01062 Dresden, Germany*
[2]*Faculty of Pharmaceutical Sciences, University of British Columbia, Vancouver, British Columbia V6T 1Z3, Canada*
[3]*Institut für Biomedizinische Technik und Informatik, Technische Universität Ilmenau, 98693 Ilmenau, Germany*
[4]*Department of Pharmaceutical Sciences, University of Maryland School of Pharmacy, Baltimore, Maryland 21201, USA*

(Received 18 May 2015; accepted 20 July 2015; published online 29 July 2015)

Microfluidic spirals were used to successfully separate rare solid components from unpretreated human whole blood samples. The measured separation ratio of the spirals is the factor by which the concentration of the rare component is increased due to the Dean effect present in a flow profile in a curved duct. Different rates of dilution of the blood samples with a phosphate-buffered solution were investigated. The diameters of the spherical particles to separate ranged from 2 μm to 18 μm. It was found that diluting the blood to 20% is optimal leading to a separation ratio up to 1.97. Using two spirals continuously placed in a row led to an increase in separation efficacy in samples consisting of phosphate-buffered solution only from 1.86 to 3.79. Numerical investigations were carried out to display the flow profiles of Newtonian water samples and the shear-thinning blood samples in the cross-section of the experimentally handled channels. A macroscopic difference in velocity between the two rheologically different fluids could not be found. The macroscopic Dean flow is equally present and useful to help particles migrate to certain equilibrium positions in blood as well as lower viscous Newtonian fluids. The investigations highlight the potential for using highly concentrated, very heterogeneous, and non-Newtonian fluidic systems in known microsystems for screening applications. © *2015 AIP Publishing LLC*. [http://dx.doi.org/10.1063/1.4927649]

I. INTRODUCTION

The separation of rare components of the blood from patients is of great importance for the disease diagnosis and its subsequent treatment. In this regard, blood screening for pathogenic bacteria[1] or circulating tumor cells (CTC)[2–4] has become of interest to the scientific community in recent years as this poses not only a scientific challenge but also holds great potential for the application in resource limited environments as a point-of-care diagnostic tool.[5] Since whole blood samples contain a high number of diverse cellular components with a concentration of about 40–45 vol. %,[6–8] separation is often either done from highly diluted or pretreated samples[2,3] or at very low volume flow rates.[9,10] With focus on point-of-care-devices, processing the blood sample prior to separation should be reduced to a minimum, while the volume flow rate should enable a reasonably high throughput.

[a)]Authors to whom correspondence should be addressed. Electronic addresses: Lisa.Sprenger@tu-dresden.de and Urs.Hafeli@ubc.ca

 © 2015 AIP Publishing LLC

Microfluidic separation devices may rely on different physical principles from the field-flow fractionation amongst which one finds sedimentation by gravity,[11] magnetophoresis,[12,13] or the Dean-effect in curved channels.[1–4,14–17] The latter is the reason for particles of certain sizes to focus in an equilibrium position in the cross-section of a microfluidic spiral. The effect was analytically described by and named after Dean[18,19] and is characterized by a cross-sectional flow consisting of two counter-rotating vortices which establish due to the curvature of the duct. In case of colloidal suspensions, the forces acting on a particle in the flow are the wall lift force, the inertial lift force, and the drag force coming from the Dean flow. If these forces, which mainly depend on the particles' diameter, but also on the fluid's viscosity and density,[15,20] balance, particles of distinct characteristics will be trapped in the cross-sectional equilibrium position close to the inner wall and will be transported along the channel by the primary flow, as schematically shown in Fig. 1. By splitting the outlet, the volumetric fraction containing those particles is separated from the flow, and the concentration of the particles in the fraction is increased compared to the initial sample.

The flow-focusing driven by the Dean-effect has been investigated by Di Carlo *et al.*[14,21–23] with the focus on describing properly the different forces involved leading to equilibrium positions of particles in a duct's cross-section. Bhagat *et al.*[15,24] concentrated on separating multidisperse particles in a number of parallel outlets. Dutz *et al.*[16,17] proved that the effect is independent from buoyancy by using magnetic particles with their density being more than twice the carrier liquid's density. Very recent investigations into using the spirals for the separation of circulating tumor cells from highly diluted or lysed blood samples by Hou *et al.*,[2] and Warkiani *et al.*[3] showed that the spirals are adequate for cancer cell extraction and that optimizing the spiral's cross-section by a trapezoidal profile leads to a more distinct separation than the rectangular one. Kim *et al.*[4] investigated the influence of various geometrical and fluidic parameters on the flow focusing effect, and proved that for a binary mixture of human leukocytes and CTCs a two step separation is an efficient way of concentrating the CTCs.

The Dean-effect is characterized by the dimensionless Dean-number[19,25,26]

$$De = \frac{\rho D_h v}{\eta}\sqrt{\frac{D_h}{2R}}, \tag{1}$$

with R denoting the radius of the channel's curvature, η the fluid's viscosity, v the mean primary flow velocity, ρ the fluid's density, and D_h the hydraulic diameter being calculated by the cross-sectional area A and the wetted perimeter P ($D_h = A/4P$). The forces present in the

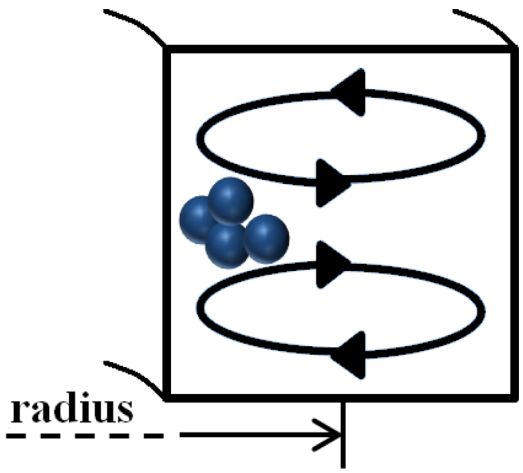

FIG. 1. Rectangular cross-section of the microfluidic spiral, the direction of the vortex-flow is marked by the depicted arrows, the equilibrium position taken by distinct particles is close to the inner channel's wall.

cross-section can be summed up in the Stokes-based Dean drag[15] and the net lift force. The Dean drag

$$F_D = 3\pi\eta v_D d_P \tag{2}$$

contains the suspension's viscosity η, the particles' size d_P, and the vortices' mean velocity v_D. The net lift force is described by[15,20]

$$F_L = \rho\dot{\gamma} C_L d_P^4, \tag{3}$$

with ρ denoting the suspension's density, the shear-rate $\dot{\gamma}$, and the lift-coefficient C_L mostly given as[15] 0.5.

Besides the force balance, the length of the spiral channel has to meet a minimum criterion to guarantee that particles while flowing with the primary flow have sufficient time to migrate to the cross-sectional equilibrium position. The minimum length of the channel, according to Bhagat *et al.*,[15] is derived from the time that a particle needs to migrate in the cross-section. This time frame, given the primary flow's velocity v leads to the channel length L by

$$L = \frac{v}{v_D} \cdot L_M, \tag{4}$$

with $L_M = D_h$ being the migration length and v_D the Dean velocity, which can be derived from Eqs. (2) and (3).

The present study aimed at investigating the efficacy of the microfluidic spirals when using a low rate of dilution of human whole blood samples. The efficacy was also tested for a continuous two-step separation device consisting of two spirals arranged in a row. Microspheres of different sizes dispersed in the blood samples were used as model system for an unspecified rare component which was to be separated from the blood. Insight gained from these investigations can then be transferred and adapted to specific tasks in separating rare solid components from a highly concentrated fluidic system. The study thereby focuses on the very basic transport phenomenon in the Dean flow being strongly influenced by hydrodynamic interactions. In addition to experiments, a numerical simulation of the flow profile in the duct was carried out considering a shear-thinning model for the blood's viscosity. The latter is presented in Section II and helps with comparing the flow profile of a Newtonian with the present non-Newtonian fluid. The experimental setup is described in detail in Section III consisting of the microfabrication process and the fluidic system under investigation.

II. SIMULATION OF FLOW PROFILE

A prerequisite of the numerical simulation of flow profile in the curved duct's cross-section is the rheological model for the fluid. It was assumed here that the fluidic properties of the carrier liquid dominate the macroscopic flow behavior, which is why the secondary flow was simulated with regards to the carrier liquid only. Simulations were carried out with water as reference fluid and whole blood as carrier liquid. Water is a Newtonian fluid with a viscosity of about 1 mPa s at room temperature.[27] Whole blood is a non-Newtonian, shear-thinning fluid. Its viscosity depends on the shear-rate applied and can be described either by the Carreau-Yasuda-model[28] or the Quemada-model.[7] The viscosity according to the first model is written as

$$\eta = \eta_\infty + (\eta_0 - \eta_\infty)(1 + (\lambda\dot{\gamma})^a)^{(n-1)/a}, \tag{5}$$

with the viscosity $\eta_\infty = 0.0035$ Pa s for an infinitely large, and $\eta_0 = 0.16$ Pa s for a vanishing shear-rate, and with the parameters $\lambda = 8.2$ s, $a = 0.64$, and $n = 0.2128$ according to Boyd *et al.*[28] The shear-rate is denoted with $\dot{\gamma}$. The viscosity according to the Quemada-model reads

$$\eta = \eta_0(1 - 0.5Hct \cdot k_Q)^{-2}, \tag{6}$$

with $\eta_0 = 0.00167\,\text{Pa s}$, and a hematocrit of $Hct = 0.45$. The intrinsic viscosity k_Q is defined by

$$k_Q = \frac{k_0 + k_\infty(\dot{\gamma}/\dot{\gamma}_c)^{0.5}}{1 + (\dot{\gamma}/\dot{\gamma}_c)^{0.5}}, \tag{7}$$

with the intrinsic viscosity $k_\infty = 1.5$ for an infinitely large and $k_0 = 4$ for a vanishing shear-rate. The critical shear-rate $\dot{\gamma}_c$ is given with $5\,\text{s}^{-1}$ according to Marcinkowska-Gapińska *et al.*[7] Comparing both models leads to the flow curves presented in Fig. 2 in the shear rate range from $0.0001\,\text{s}^{-1}$ to $100\,000\,\text{s}^{-1}$. For very low shear-rates, the models predict a fluid being about 150 times more viscous than water, while for shear-rates above $1000\,\text{s}^{-1}$ the blood is described as being only 3 to 4 times more viscous than the reference fluid.

The numerical simulation of the flow in the curved duct was carried out with Fluent (ANSYS, Inc., Canonsburg, PA, USA). To solve the steady-state formulation of the equations of motion of the flow, a pressure-based laminar solver is used. The inlet is modeled as a velocity inlet, where the mean velocity on the cross-section is set. The outlet is modeled as pressure outlet, with no pressure beyond the ambient pressure being applied. The channel walls are impermeable, and the no-slip condition applies. The blood's viscosity is introduced by a user-defined-function (UDF), and since the Quemada- and the Carreau-Yasuda-models lead to very similar results, the first one is chosen for the simulations implementing a hematocrit of 45%. The solution is calculated on a five quarter circle, see Fig. 3. The inlet is positioned at 90°, the outlet at 180° at a radius of 6 mm. The geometry is discretized at roughly 1.4×10^6 nodes with hexahedral mesh elements, with a uniform node to node spacing.

To achieve a valid comparison of water and blood flowing through the duct, the Reynolds number

$$Re = \frac{\rho D_h v}{\eta}, \tag{8}$$

with ρ being the fluid's density, η its viscosity, D_h being the characteristic length scale, and v the fluid's mean velocity must be equal in both cases. Since the blood's viscosity is approximately the fourfold of the water's viscosity, the velocity is also assumed to be fourfold. To emphasize the Dean effect in the flow, the mean velocity for the water simulation is set to 5 m/s, while the velocity for blood is chosen to be 20 m/s. These values are merely used for comparison of the Dean effect in the two rheologically different fluids. The high velocity does not have a relevance in the experiments conducted and described in Sec. III. Fig. 4(a) depicts the flow profile in water, while 4(b) presents the blood's flow profile. The Dean-effect can be identified

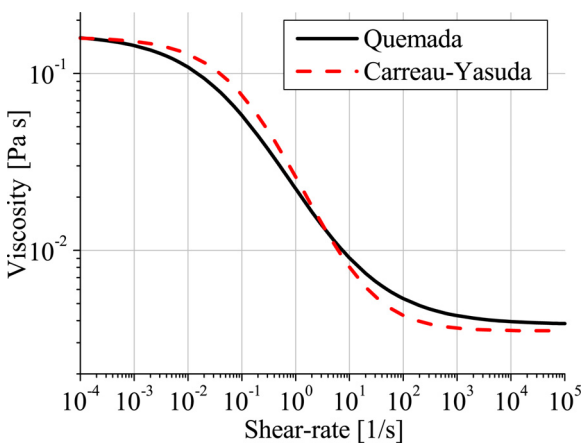

FIG. 2. Viscosity is presented here in dependence on the shear-rate for the Carreau-Yasuda-blood-model (dashed red line) and the Quemada-blood-model (solid black line).

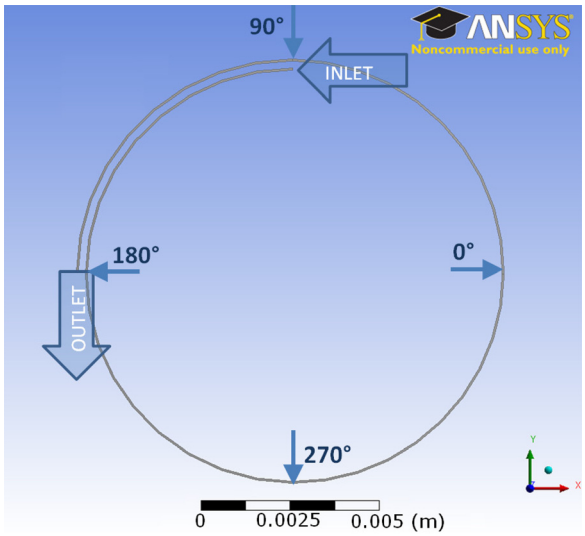

FIG. 3. Geometry used for simulations in Fluent (ANSYS, Inc., Canonsburg, PA, USA).

by the presence of a secondary flow profile, which is depicted by the arrows. A two-dimensional cross-sectional flow with a maximum of 0.24 m/s (water) and 0.94 m/s (blood) establishes due to the curvature of the duct. The maximum primary flow (color mapped), characterized by a parabolic profile in straight ducts, is shifted to the outer wall of the duct, resulting in a cross-sectional pressure gradient which drives the secondary flow. The maximum velocity along the duct is approximately two times the mean inlet velocity in both fluids. Fig. 4 emphasizes that the Dean-effect is equally present in both water and blood, which are rheologically rather different fluids.

The relevant question for the experiments is the order of magnitude of the shear rate, since it directly influences the fluid's viscosity. Fig. 5 presents the shear rate over the cross-section's width at 180° at different heights in the channel, when blood flows through the duct at a mean velocity of (a) 0.3 m/s and (b) 1.6 m/s. All simulated values are larger than $700\,s^{-1}$ which, if considering Fig. 2, stresses the fact that the shear in the cross-section should most likely evoke a Newtonian behavior of the blood. The Dean-effect is thereby a reasonable *Ansatz* for separating particles from blood flow in microfluidic spirals. The numerical treatment of the interaction between solid cellular components of the blood and the experimentally dispersed particles to separate has to be considered as a highly complex numerical task which cannot be addressed within the present work.

III. EXPERIMENTAL SETUP

A. Design parameters of the microfluidic spirals

The design of the microfluidic spirals is bound to several constraints concerning flow and geometry. Di Carlo *et al.*[14] found out that focusing of particles is only possible if the relative particle size d_P/D_h exceeds 0.07, while the Dean number De should be larger than 1. At the same time, the minimum length of the spiral has to be respected to enable particles to migrate across the channel's cross-section while being transported along the duct by the primary flow. A constraint for the volume flow rate comes from the polymer used to fabricate the channels. Previous investigations[17] suggest a maximum flow rate of about 100 μl/min–150 μl/min, otherwise the high pressure inside the channels leads to a rupture of the bond between the two polymer pieces that form the channel or to a deformation of the cross-section leading to a reduction in efficacy of the flow focusing.[4] The last condition concerns the multiple step separation. If keeping the cross section constant along different steps of separation, a bisection of the volume flow rate from one spiral to the following is the result. The Dean number

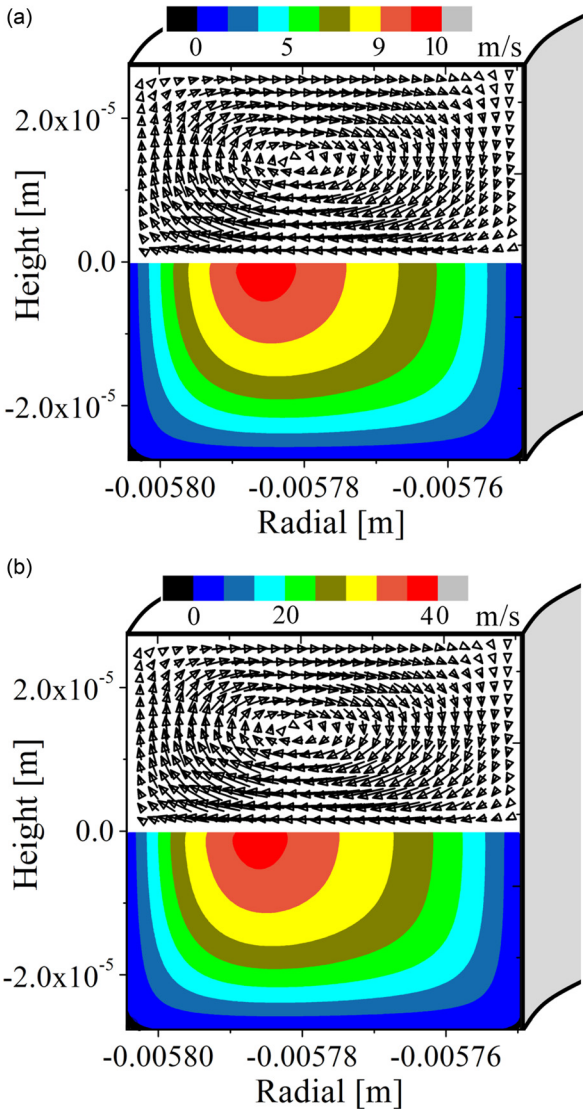

FIG. 4. Primary (color mapped) and secondary (arrows) flow profile in the duct's cross-section at 180°. Rheological models for (a) water and (b) blood were applied. The mean inlet velocity was chosen to be (a) 5 m/s and (b) 20 m/s for matching Reynolds numbers.

$$De = \frac{\rho D_h v}{\eta}\sqrt{\frac{D_h}{2R}} \tag{9}$$

is then also bisected, unless the spiral's radius R is adapted. The channel's height and width are chosen to be approximately 50 μm for particle sizes from 6 to 15 μm. For those reasons, the basic spirals radii are chosen to be 6 mm, 4 mm, 2.5 mm, and 2 mm with respective volume flow rates in the range of 100–150 μl/min in the large, 50–75 μl/min in the medium, and 25–30 μl/min in the small spiral.

B. Microfabrication

The microfluidic chips were made from polydimethylsiloxane (PDMS, Sylgard184, DowCorning, Midland, MI, USA) which was cast from a mold containing the negative image of the spirals' structure. The mold was prepared by layering a silica wafer with a negative photoresist (SU-8 2075, Microchem, Newton, USA). The layer's thickness determines the channel's

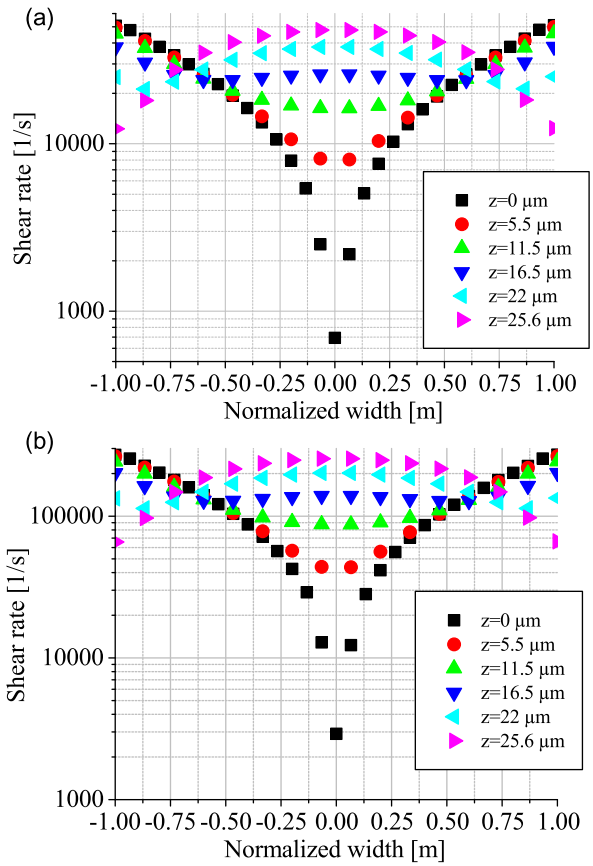

FIG. 5. Shear-rate across the duct's width at 180°. The mean inlet velocity is (a) 0.3 m/s and (b) 1.6 m/s.

height. The exposure of the photoresist to UV-light triggers cross-linking processes which hardens the polymer. A transparency sheet was used as mask (CAD/Art Services, Bandon, USA) to project the channel's structure onto the photoresist during exposure. After casting and curing, the PDMS (10 parts base, 1 part curing agent) was peeled off the mold, the in- and outlet ports were created by hole punchers, and the chips were catalyst bond onto glass slides by dipping the PDMS tiles into the polymer's curing agent before placing them onto the slides.[29] In a prior step, the glass slides were coated with PDMS (3 parts base, 1 part curing agent).

The experiments that we conducted can be divided into two different stages, both aiming at designing a multiple-step chip with two to three spiral channels placed in a row. Each spiral's outlet was split into two equal fractions, the inner one assumingly carrying the microspheres, see Fig. 6.

The first experimental stage focused on individual spirals with radii of 6 mm, 4 mm, 2.5 mm, and 2 mm for the outer turn, and using three different volume inflow rates each. The second stage aimed at optimizing the channel's length and interconnecting spirals of radii of 6 mm and 4 mm. The rectangular cross-section was 55 μm wide and either 65 μm or 47 μm high, leading to a hydraulic diameter of either 60 μm or 51 μm, respectively. The channels' lengths were approximated by the length of all turns using the mean radius of the spiral, the outflow channel was considered as radius of the outer turn. The specific geometric parameters are summed up in Table I.

C. Fluidic system

The carrier liquid of the fluidic samples investigated within this work consisted of phosphate buffered saline with 2 mM ethylenediaminetetraacetic acid (99.4%–100.06%, Cat. No. E9884; Sigma Aldrich, Inc., St. Louis, MO, USA) and 0.5% bovine serum albumin (FractionV,

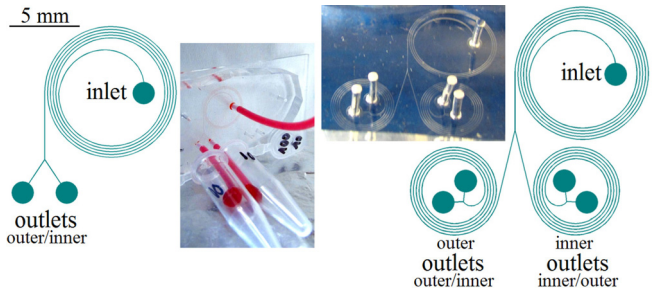

FIG. 6. On the left: drawing of the individual spiral, in- and outlet ports are marked. On the right: drawing of the two-step separation chip with the identification of the in- and outlet ports, including their labels.

approximately 99%; Cat. No. A3059; Sigma Aldrich, Inc., St. Louis, MO, USA), ($c_b = 0$) or buffer and human whole blood mixtures of 20% blood ($c_b = 0.2$) or more ($c_b > 0.2$). The rare component to separate from the carrier liquid was represented by glass ($\rho_{gl} = 2200\,\text{kg/m}^3$) and polystyrene microspheres ($\rho_{ps} = 1000\,\text{kg/m}^3$, micromer®, micromod Partikeltechnologie, Germany) of different sizes from 2 μm to 18 μm which were separately dispersed in samples of approximately 1.5 ml. Buoyancy in the case of glass spheres due to the difference in density of the carrier liquid and the particles can be neglected, since former investigations of Dutz *et al.*[17] revealed that the separation by the Dean effect is not affected by buoyancy. The number of the particles in the samples was kept constant throughout the experiments and was determined to approximately 350 particles/μl, while the minimum number of red blood cells ($c_b = 0.2$) was approximately 10^6 cells/μl.

The particles' sizes were determined by a light scattering method with the Mastersizer Hydro 2000SM (Malvern Instruments Ltd, Worcestershire, UK). The particle size distribution is presented in Fig. 7 as cumulative frequency in dependence from the particles' diameters. The average diameter $d50$ is obtained by the measurements and leads to individual particle sizes of 2.4 μm, 6.8 μm, 9.7 μm, and 18.1 μm. The specific fluidic parameters are summed up in Table II. The parameters were used in the following to determine the Dean number, the dimensionless diameter as quotient of the particle size d_p, and the channel's hydraulic diameter D_h.

D. Experimental procedure

The samples of 1.5 ml were mixed right before carrying out the experiment. The whole blood samples were never older than five days after donation. A potential degeneration of the cellular content was thereby reproducibly kept low, and aging effects of the samples did not influence the experimental output. The samples were additionally kept cool, and in evacuated and EDTA coated vials. After mixing, the inlet sample was pushed through the chip by a syringe pump. The volume rate used depended on the radius of the spiral channel (see Table III). The samples at the outlets flowed into microcentrifuge tubes. They were either analyzed directly or diluted with DI water first to facilitate the identification and the counting of the particles. To minimize problems with sedimentation of the solid components in the inlet sample, the syringe pump was positioned vertically and the experimental run-time was kept short (mostly 2–4 min).

TABLE I. Design parameters of the microfluidic spirals for separation.

Radius (outer turn) (mm)	6.0	4.0	2.5	2.0
Height (μm)	47; 65			
Width (μm)	55		35; 55	
Spacing between turns (μm)	200			150
Number of turns	3.5; 5.5		5.5	
Approx. length (mm)	132; 196	125	75	60

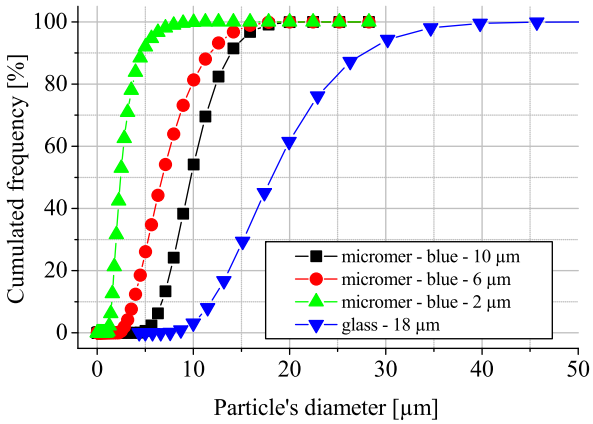

FIG. 7. Particle size distribution of four different samples of particles from 2 μm to 18 μm in diameter.

TABLE II. Relevant parameters of the fluidic system which are used to approximate experimental numbers, such as the Dean number, or the dimensionless diameter.

Carrier liquid	Water	Whole blood
Density (kg/m^3)	1000	1200
Viscosity (Pa s)	0.001	0.004
Particles	**Polystyrene**	**Glass**
$d10$ (μm)	1.5; 3.8; 6.8	11.9
$d50$ (μm)	2.4; 6.8; 9.7	18.1
$d90$ (μm)	4.7; 11.7; 13.8	27.6

The specific parameters for carrying out the experiments with single spirals are summed up in Table III. Experiments with the two-step separation were all carried out at an inflow rate of 100 μl/min, at concentrations of either $c_b = 0$ or $c_b = 0.2$, and with particles of the size of $d50 = 6.8$ μm or $d50 = 9.7$ μm.

The evaluation of the efficacy of the experiments is described by the separation ratio (also known as "enrichment ratio")

$$s_r = \frac{c_{io}}{c_{av}} = \frac{c_{io}}{\frac{V_{io}}{V_t} c_{io} + \frac{V_{oo}}{V_t} c_{oo}}, \tag{10}$$

with $c_{io(oo)}$ being the concentration of particles in the inner (outer) outlet and $V_{io(oo)}$ being the volume obtained at the inner (outer) outlet. The total volume at the outlets as sum of V_{io} and V_{oo} is denoted V_t. The individual volumes at the outlets were measured with a pipette, while the particle concentrations were determined by counting particles using a hemocytometer. The particle count for each experiment was done with at least two different samples per outlet

TABLE III. Parameters for setting up the experiments with single spirals.

Radius (outer turn) (mm)	6.0	4.0	2.5	2.0
Volume flow (μl/min)	150; 100; 50	75; 50; 25	25; 10; 8	
Time (min)	2–3	3–8	8–10	
Concentration c_b	0; 0.2; 0.5		0; 0.2	0.2
Particle size (μm)	6.8; 9.7; 18.1	2.4; 6.8; 9.7; 18.1	6.8; 9.7; 18.1	6.8; 9.7

fraction, and 200–1000 particles per experiment were counted. The results obtained from the experimental studies described here are presented in Section IV including their discussion.

IV. RESULTS AND DISCUSSION

The results and discussion are subdivided into a first section concerning the single spirals' experiments and a second section about the multiple-step spirals.

A. Single spirals

The use of different solvents and/or particle concentrations in our spirals leads to different efficacies of particle separations (Fig. 8). The experimental results are separately presented for buffer-only ($c_b = 0$) and blood-carrying ($c_b > 0$) samples in Figs. 8(a) and 8(b). The experiments are characterized by the Dean number resulting from the geometric and fluidic parameters of each experimental run and the relative particle size (d_p/D_h). The color mapping of the individual symbols represents the efficacy of the separation by the separation ratio s_r. Since the splitter of the outlet port splits the flow in half, the theoretical maximum separation ratio is 2. The splitter depends on the exact geometry of the outlets and the pressure in the fluid. If the geometry of the two outlet ports in the experiments slightly varies or a cross-sectionally inhomogeneous distribution of the blood cells is present, the fractions' volumes might as well slightly differ then potentially leading to larger values than $s_r = 2$. The black dashed lines mark

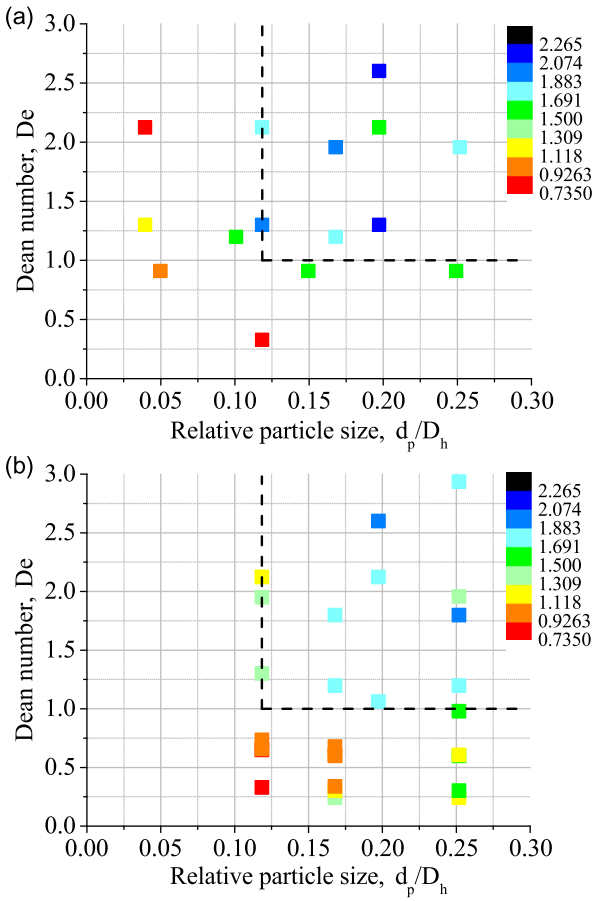

FIG. 8. Separation ratio s_r (color mapping) is presented while categorizing the experiments by the Dean number and the relative particle size (d_p/D_h). (a) Carrier liquid is the phosphate-buffered solution ($c_b = 0$); (b) carrier liquid contains human whole blood and the phosphate-buffered solution ($c_b > 0$). Left of and below the dashed lines separation is rated as insufficient.

the area where separation of the particles from the sample is regarded to be successful. The Dean number is larger than 1.00 in this area while the relative particle size is larger than 0.12. For the blood-free samples, the efficacy for those parameters ranged from 1.69 to 2.19. Fig. 8(b) depicts the separation ratios for the blood-containing samples, where most of the samples were prepared as one part blood with four parts buffered carrier liquid ($c_b = 0.2$). The efficacy of separation for $De > 1.00$ and $d_p/D_H > 0.12$ was 1.34 in its minimum and 1.97 in the maximum. The decrease in efficacy results from the number of blood cells present in the sample. Assuming a hematocrit of 45% still leaves the diluted sample with not less then 9% cellular components, and a concentration of red blood cells (RBC) of approximately 10^6 cells/μl. It is especially this high concentration of RBCs that influences the establishment of the Dean vortices and the cross-sectional migration of the spherical particles. Due to hydrodynamic interaction between cells and particles, the efficacy of the separation process is diminished. A second reason for the decrease in efficacy can be found in the size of the RBCs. With a diameter of approximately 6–8 μm in their disk-like direction,[8] they might also tend to migrate across the cross-section, and keep spherical particles out. Further experimental investigations have to focus on shape-specific separation properties for spheres, rods, disks, etc.

With an increase in the relative particle size and for Dean numbers exceeding 1.00, the separation efficacy can also be increased in dependence of the sample's blood concentration, as summed up in Fig. 9, where the separation ratio is presented depending on the relative particle size. The filled symbols are mean values for the separation efficacy averaged over all experiments conducted for the specific relative particle size where the Dean number exceeds 1.00. The corresponding open symbols stand for the experiments with Dean numbers smaller than 1.00, which were rated as "failing separation purposes" by considering Fig. 8. The error bars in Fig. 9 represent the deviation from the average value throughout the experiments. Fig. 9 supports the idea of dividing the experimental results into two categories by their respective Dean number, which means that the fluid's primary velocity, its viscosity, density, and the channel's geometry have to meet certain criteria to enable the separation of the particles taking place. Still there is a dependence of the efficacy on the relative particle size emphasizing that very small particles cannot be focused in an equilibrium position, and separation therefore fails. The last aspect drawn from the figure is the blood concentration. A large number of experiments containing 20% of whole blood were conducted and were found to be still reasonably successful, while higher concentrations led to less efficient separation, and experimental challenges such as the pressure along the channel.

To further increase the efficacy in only one separation step, a geometrically asymmetric splitter leading to the outlet ports was tested. Generally speaking, the volume flow in a channel can be linked to the pressure difference between the channel's inlet and outlet by[30]

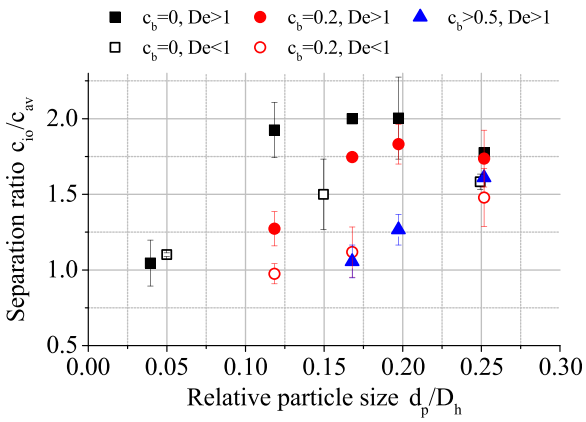

FIG. 9. Separation efficacy in dependence from the relative particle size, where ● and ▲ stand for blood containing samples, while ■ represents bloodless samples. Open symbols depict mean efficacy of experiments run with Dean numbers being smaller than 1.00, while filled symbols represent those with Dean numbers exceeding 1.00.

$$\Delta p = R\dot{V}, \tag{11}$$

where $\dot{V}$ denotes the volume flow, Δp the pressure difference between inlet and outlet of the channel, and R the fluidic resistance. The latter depends on the channel's geometry, and can be written as[9,30,31]

$$R = \frac{12\eta l}{h^3 w}\left(1 - 6\frac{h}{w}\sum_{n=1}^{\infty}\left[\lambda_n^{-5}\tanh\left(\lambda_n\frac{w}{h}\right)\right]\right)^{-1} \tag{12}$$

for rectangular channels if the height h is shorter than the width w (if $h > w$: symbols are accordingly switched in Eq. (12)). The length of the channel is denoted by l, the fluid's viscosity by η, and $\lambda_n = (2n+1)/2\pi$. Since multiple heights in the same microfluidic spiral cannot be easily achieved, it is either the shorter length or a narrower width that leads to an increase in resistance in the inner of the two outlets. Since the pressure drop along both outlet channels is identical, the increase in resistance leads to a reduction in the volume flow. If the particles still flow with the inner fraction, their concentration can be increased in comparison with the symmetric splitter. The outlets were designed with a width for the inner outlet of 40 μm, while the outer was kept at 55 μm. The experimental results for spirals of a radius of 6 mm, with 3.5 windings, an inflow rate of 100 μl/min, and particles of the size of 6 μm dispersed in the buffer solution are presented in Fig. 10. The squares represent different experimental runs with the symmetric splitter for the given relative particle size d_p/D_h. The circles belong to the experiments with the asymmetric splitter. The mean efficacy of $s_r = 1.86^{+0.28}_{-0.34}$ was increased to $2.25^{+0.26}_{-0.16}$, where the deviations represent the experimental span of the separation ratio. A relative increase in the efficacy by roughly 21% was gained by changing the splitter's geometry. The reason for a lower increase in separation efficacy than expected theoretically is to be searched for in the stream splitting surfaces[12,32] caused by the splitter itself. While a symmetric splitter leads to symmetric flow rates towards the outlet ports, asymmetric flow rates lead to asymmetric splitting surfaces in the vicinity of the splitter.[12,32] These splitting surfaces influence the flow rate towards the outlets so that the theoretical increase in fluidic resistance as given above does not lead to an according decrease in the experimental flow rate. If the equilibrium position of the focused particles deviates a little, the particles might even bounce to the outer outlet. If carrying out systematic studies for the splitter geometry, these splitting surfaces have to be modeled according to theoretical ideas of Giddings and Williams.[32]

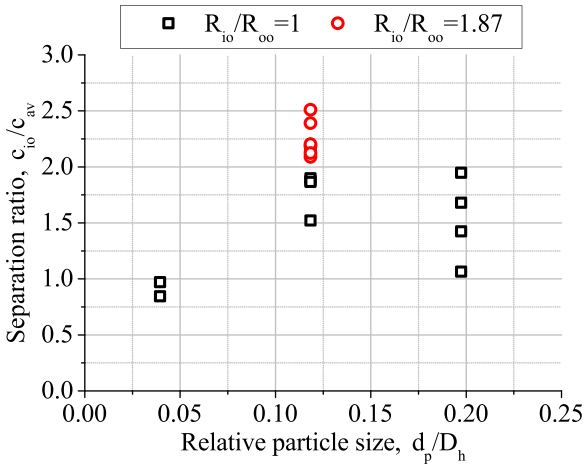

FIG. 10. Separation efficacy in dependence from the relative particle size, the different symbols denote the symmetric (□) and asymmetric (◦) splitting of the outlet port.

B. Two-step spirals

In a second stage of the experimental investigations, the larger two of the aforementioned single spirals was continuously connected (see Fig. 6). The inlet port for the system was placed in the center of a spiral of 6 mm in radius and 3.5 windings. The last winding was split into two equal channels, keeping the cross-sectional geometry. These two channels represented the inlet for the following spirals, 4 mm in radius each, and with a length of 5 windings. Each outlet of these spirals was again split into two equal outlet ports. The smaller spirals were identical, and positioned mirrored to each other to keep the fluidic resistance in both spirals identical, resulting in identical volume flow rates. The configuration offers the opportunity to determine the separation ratio for the larger spiral, as well as the follow-up separation ratios of the smaller spirals separately and the one only regarding the concentration of the inner outlet port of the inner 4 mm spiral. Fig. 11 presents what is gained from this two-step separation. Fig. 11 depicts the experimental result of samples not containing blood as separation ratio depending on the relative particle size, where ◦-symbols stand for the separation ratio determined by the outlet concentration of the inner 4 mm-spiral's inner outlet and the average inlet concentration. The □-symbols represent the separation efficacy of each spiral individually with regard to the average concentration of the single spirals determined by the concentrations of inner and outer outlet port. Fig. 11 presents the experimental results of samples containing 20% of whole blood with the same scheme.

Concentrating on the buffer-only samples in Fig. 11 points out that the one step separation in these spirals led to an averaged efficacy of the process of 1.87 for particles of $d_p/D_h \approx 0.2$, and to 1.95 for $d_p/D_h \approx 0.12$. With the determination of the overall efficacy of both steps, the efficacy was increased by a factor of 2–3.79 in the first and by 1.9–3.63 in the second case when comparing the inlet concentration with the concentration at the inner fraction of the inner 4 mm-spiral. Looking at Fig. 11 shows that this behavior cannot be found with the blood-containing samples. Their handling was quite challenging. Applying the same volume flow rates as in the case of the buffer solution, the pressure along the channel, if using blood containing samples, as shown in Eqs. (11) and (12), increases significantly due to the rheological behavior of the blood samples. While the rheological behavior of the blood did not cause severe problems in the single spirals with approximate duct-lengths of 120 mm–130 mm, the influence on the pressure in the two-step spirals with an approximate length of 240 mm often caused the spirals to collapse. The small number of successfully conducted experiments showed that an increase in separation efficacy up to around 2.6 was possible in the two-step configuration. This value corresponds to an efficacy of 1.6 in each step, which is reasonable with regard to Fig. 9.

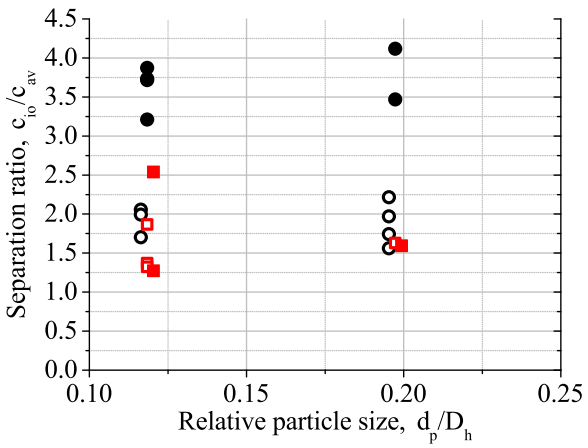

FIG. 11. Separation ratio of single spirals s_r (open symbols) and two-step spirals (filled symbols) in relation to their relative particle size (d_p/D_h). The used carrier liquid was phosphate-buffered solution ($c_b = 0$) (black circles) or diluted human whole blood ($c_b > 0$) (red squares).

The continuous two-step procedure in the present configuration cannot be applied to the separation purpose reasonably.

V. CONCLUSIONS

Separation of solid spherical particles from samples containing up to 20% human whole blood led to a particle enrichment factor of 1.97. The two-step separation process in a blood-free sample resulted in the expected increase in separation efficiency from a factor 2–3.8. However, samples containing blood were difficult to handle in the two-step setup, and did not lead to a significant improvement in separation.

The two experimental main challenges linked with the separation from blood samples were hydrodynamic interactions between cells and the rare components as well as the blood-sample's viscosity. The hydrodynamic interactions were very complex since the order of magnitude of all components contained in the system was identical. Only RBCs alone tend to interact strongly, an interaction with the solid spherical particles can therefore be expected. Further numerical and experimental work might shed light on different regimes of interactions, and their influence on the flow field. Regarding rheological properties, the blood-containing samples were more viscous than the buffered carrier liquid resulting in a significant increase in pressure at the channel's inlet. Even focusing on a minimum length for the two-step spirals, the inlet pressure, needed to flow the sample through the chip, quite regularly led to a collapse of the channel. Future, experimental and numerical work has to be focus on the determination of the critical pressure leading to that collapse. Nonetheless, separation from moderately diluted whole blood samples by Dean flow is a promising method.

ACKNOWLEDGMENTS

Financial support by a fellowship of the German Academic Exchange Service (DAAD), a grant from the Natural Sciences and Engineering Research Council (NSERC) in Canada, support of micromod Partikeltechnologie GmbH, Rostock, Germany, by providing particles, and support by Professor Christoph Alexiou (Universitätsklinikum Erlangen, Germany) and Dr. Boris Stöber (UBC Vancouver, Canada) are gratefully acknowledged.

[1]W. Lee, D. Kwon, W. Choi, G. Y. Jung, and S. Jean, "3D-printed microfluidic device for the detection of pathogenic bacteria using size-based separation in helical channel with trapezoid cross-section," Sci. Rep. **5**, 7717 (2015).
[2]H. W. Hou, M. E. Warkiani, B. L. Khoo, Z. R. Li, R. A. Soo, D. S.-W. Tan, W. T. Lim, J. Han, A. A. S. Bhagat, and C. T. Lim, "Isolation and retrieval of circulating tumor cells using centrifugal forces," Sci. Rep. **3**, 1259 (2013).
[3]M. E. Warkiani, G. Guan, K. B. Luan, W. C. Lee, A. A. S. Bhagat, P. K. Chaudhuri, D. S.-W. Tan, W. T. Lim, S. C. Lee, P. C. Y. Chen, C. T. Lim, and J. Han, "Slanted spiral microfluidics for the ultra-fast, label-free isolation of circulating tumor cells," Lab Chip **14**, 128–137 (2014).
[4]T. H. Kim, H. J. Yoon, P. Stella, and S. Nagrath, "Cascaded spiral microfluidic device for deterministic and high purity continuous separation of circulating tumor cells," Biomicrofluidics **8**, 064117 (2014).
[5]H. Esmaeilsabzali, T. V. Beischlag, M. E. Cox, A. M. Parameswaran, and E. J. Park, "Detection and isolation of circulating tumor cells: Principles and methods," Biotechnol. Adv. **31**, 1063–1084 (2013).
[6]E. W. Merrill, "Rheology of blood," Physiol. Rev. **49**, 863–888 (1969).
[7]A. Marcinkowska-Gapińska, J. Gapinksi, W. Elikowski, F. Jaroszyk, and L. Kubisz, "Comparison of three rheological models of shear flow behavior studied on blood samples from post-infarction patients," Med. Biol. Eng. Comput. **45**, 837–844 (2007).
[8]Y.-C. Fung, *Biomechanics - Mechanical Properties of Living Tissues* (Springer Science + Business Media, 2004).
[9]P. Sethu, A. Sin, and M. Toner, "Microfluidic diffusive filter for apheresis (leukapheresis)," Lab Chip **6**, 83–89 (2006).
[10]K. I. Byun, H. C. Bang, H. J. Kim, E. D. Han, Y. H. Seo, and B. H. Kim, "Blood separation device based on microstructures in microchannels," in *4th International Conference on Biomedical Engineering in Vietnam IFMBE Proceedings* (Springer Berlin Heidelberg, 2013), Vol. 40, pp. 161–164.
[11]J. Bertrand, B. Liagre, G. Bégaud-Grimaud, M. O. Jauberteau, J. L. Beneytout, P. Cardot, and S. Battu, "Analysis of relationship between cell cycle stage and apoptosis induction in K562 cells by sedimentation field-flow fractionation," J. Chromatogr. B **877**, 1155–1161 (2009).
[12]T. Schneider, S. Karl, L. R. Moore, J. J. Chalmers, and P. S. W. Zborowski, "Sequential CD34 cell fractionation by magnetophoresis in a magnetic dipole flow sorter," Analyst **135**, 62–70 (2010).
[13]M. Zborowski, *Magnetic Cell Separation*, edited by M. Zborowski and J. J. Chalmers (Elsevier Amsterdam, 2007), p. 105.
[14]D. Di Carlo, D. Irimia, R. G. Tompkins, and M. Toner, "Continuous inertial focusing, ordering, and separation of particles in microchannels," Proc. Natl. Acad. Sci. U.S.A. **104**, 18892–18897 (2007).

[15]A. A. S. Bhagat, S. S. Kuntaegowdanahalli, and I. Papautsky, "Continuous particle separation in spiral microchannels using dean flows and differential migration," Lab Chip **8**, 1906–1914 (2008).
[16]S. Dutz, M. E. Hayden, A. Schaap, B. Stoeber, and U. O. Häfeli, "Fractionation of magnetic microspheres for magnetic drug targeting using Dean flow combined with a magnetic octupole on a chip," in 15th International Conference on Miniaturized Systems for Chemistry and Life Sciences, 2011.
[17]S. Dutz, M. E. Hayden, A. Schaap, B. Stoeber, and U. O. Häfeli, "A microfluidic spiral for size-dependent fractionation of magnetic microspheres," J. Magn. Magn. Mater. **324**, 3791–3798 (2012).
[18]W. R. Dean, "Note on the motion of fluid in a curved pipe," Philos. Mag. (Ser. 7) **4**, 208–223 (1927).
[19]W. R. Dean, "The stream-line motion of fluid in a curved pipe (second paper)," Philos. Mag. (Ser. 7) **5**, 673–695 (1928).
[20]E. S. Asmolov, "The inertial lift on a spherical particle in a plane Poiseuille flow at large channel Reynolds number," J. Fluid Mech. **381**, 63–87 (1999).
[21]D. Di Carlo, J. F. Edd, D. Irimia, R. G. Tompkins, and M. Toner, "Equilibrium separation and filtration of particles using differential inertial focusing," Anal. Chem. **80**, 2204–2211 (2008).
[22]D. Di Carlo, "Inertial microfluidics," Lab Chip **9**, 3038–3046 (2009).
[23]D. Di Carlo, J. F. Edd, K. J. Humphry, H. A. Stone, and M. Toner, "Particle segregation and dynamics in confined flows," Phys. Rev. Lett. **102**, 094503 (2009).
[24]S. S. Kuntaegowdanahalli, A. A. S. Bhagat, G. Kumar, and I. Papautsky, "Inertial microfluidics for continuous particle separation in spiral microchannels," Lab Chip **9**, 2973–2980 (2009).
[25]S. A. Berger, L. Talbot, and L.-S. Yao, "Flow in curved pipes," Annu. Rev. Fluid Mech. **15**, 461–512 (1983).
[26]A. P. Sudarsan and V. M. Ugaz, "Multivortex micromixing," Proc. Natl. Acad. Sci. U.S.A. **103**, 7228–7233 (2006).
[27]H. Barnes, J. F. Hutton, and K. Walters, *An Introduction to Rheology* (Elsevier, Oxford, 2005).
[28]J. Boyd, J. M. Buick, and S. Green, "Analysis of the Casson and Carreau-Yasuda non-Newtonian blood models in steady and oscillatory flows using the lattice Boltzmann method," Phys. Fluids **19**, 093103 (2007).
[29]B. Samel, M. K. Chowdhury, and G. Stemme, "The fabrication of microfluidic structures by means of full-wafer adhesive bonding using a poly(dimethylsiloxane) catalyst," J. Micromech. Microeng. **17**, 1710–1714 (2007).
[30]H. A. Stone, *CMOS Biotechnology*, edited by H. Lee, D. Ham, and R. M. Westervelt (Springer Science+Business Media, LLC, New York, 2007).
[31]M. J. Fuerstmann, A. Lai, M. E. Thurlow, S. S. Shevkoplyas, H. A. Stone, and M. Whitesides, "The pressure drop along rectangular microchannels containing bubbles," Lab Chip **7**, 1479 (2007).
[32]J. C. Giddings and P. S. Williams, "Fractionating power in programmed field-flow fractionation: Exponential sedimentation field decay," Anal. Chem. **59**, 28–37 (1987).